Two-dimensional imaging of edge-localized modes in KSTAR plasmas unperturbed and perturbed by n=1 external magnetic fields

G. S. Yun, W. Lee, M. J. Choi, J. Lee, H. K. Park, C. W. Domier, N. C. Luhmann Jr., B. Tobias, A. J. H. Donné, J. H. Lee, Y. M. Jeon, S. W. Yoon, and KSTAR team

Citation: Physics of Plasmas (1994-present) **19**, 056114 (2012); doi: 10.1063/1.3694842
View online: http://dx.doi.org/10.1063/1.3694842
View Table of Contents: http://scitation.aip.org/content/aip/journal/pop/19/5?ver=pdfcov
Published by the AIP Publishing

Two-dimensional imaging of edge-localized modes in KSTAR plasmas unperturbed and perturbed by n=1 external magnetic fields[a)]

G. S. Yun,[1,b)] W. Lee,[1] M. J. Choi,[1] J. Lee,[1] H. K. Park,[1] C. W. Domier,[2] N. C. Luhmann, Jr.,[2] B. Tobias,[3] A. J. H. Donné,[4,5] J. H. Lee,[6] Y. M. Jeon,[6] S. W. Yoon,[6] and KSTAR team
[1]*Pohang University of Science and Technology, Pohang 790-784, South Korea*
[2]*University of California at Davis, Davis, California 95616, USA*
[3]*Plasma Physics Laboratory, Princeton University, Princeton, New Jersey 08543, USA*
[4]*FOM-Institute for Plasma Physics Rijnhuizen, 3430 BE Nieuwegein, The Netherlands*
[5]*Einhoven University of Technology, 5600 MB Einhoven, The Netherlands*
[6]*National Fusion Research Institute, Daejeon 305-333, South Korea*

(Received 9 December 2011; accepted 14 February 2012; published online 5 April 2012)

The temporal evolution of edge-localized modes (ELMs) has been studied using a 2-D electron cyclotron emission imaging system in the KSTAR tokamak. The ELMs are observed to evolve in three distinctive stages: the initial linear growth of multiple filamentary structures having a net poloidal rotation, the interim state of regularly spaced saturated filaments, and the final crash through a short transient phase characterized by abrupt changes in the relative amplitudes and distance among filaments. The crash phase, typically consisted of multiple bursts of a single filament, involves a complex dynamics, poloidal elongation of the bursting filament, development of a fingerlike bulge, and fast localized burst through the finger. Substantial alterations of the ELM dynamics, such as mode number, poloidal rotation, and crash time scale, have been observed under external magnetic perturbations with the toroidal mode number $n = 1$. © *2012 American Institute of Physics*. [http://dx.doi.org/10.1063/1.3694842]

I. INTRODUCTION

High-confinement mode (*H*-mode) in tokamak plasmas, a promising operation mode for future burning plasma devices such as ITER, relies on an edge transport barrier for confinement enhancement.[1] The transport barrier region (also called *pedestal*) is prone to the filamentary perturbations called edge localized modes (ELMs) (Ref. 2) due to the excess pressure built in that region. Understanding and control of the ELMs are considered essential for impurity transport and safety of the first wall in *H*-mode based operations because the ELM instabilities are terminated with a rapid ejection of the pedestal particles and heat onto localized regions of the first wall. In particular, the heat load on the impacted wall, projected to be up to tens of MJ per event on ITER, can be detrimental well beyond the tolerable limit of the wall material.[3]

The onset and subsequent evolution of ELMs have been investigated extensively since the discovery of *H*-mode. The observed onset thresholds of ELMs are generally in good agreement with theoretical predictions based on linear magnetohydrodynamic (MHD) instabilities, i.e., pressure-driven ballooning modes modified by current-driven kink modes.[4] Substantial details of ELM dynamics have also been revealed experimentally in multiple tokamaks:[5–10] (1) prior to the crash, the ELMs are filamentary perturbation of the electron density formed along the local magnetic field lines in the pedestal, (2) during the crash phase, the ELM filaments suddenly detach or burst at different times from the pedestal and expand radially into the scrape-off layer (SOL), and (3) the ELM crash induces a rapid ejection of heat and particles from the pedestal out to the SOL.

During recent experiments in the KSTAR tokamak,[11] the details of the entire ELM evolution process have been observed in real-time 2D images via a 2D electron cyclotron emission imaging (ECEI) system,[12] revealing nonlinear and nonuniform nature of the ELM growth and burst process with sufficient temporal and spatial resolutions.[13] This paper summarizes the ELM dynamics observed in typical KSTAR *H*-mode plasmas and reports new observations on altered ELM dynamics under external magnetic perturbations following a brief introduction of the KSTAR ECEI system.

II. ELECTRON CYCLOTRON EMISSION IMAGING IN KSTAR

The ECEI is a 2D extension of the established radiometry for the local measurements of electron cyclotron emission (ECE) intensity (T_{rad}), which is proportional to the electron temperature (T_e) in optically thick plasmas.[14] The ECEI systems recently launched in multiple tokamaks have provided high-resolution 2D T_e fluctuation images inside the tokamak plasmas where the optical depth (τ) for ECE is large ($\tau > 1$), making substantial contributions to the physics understanding of sawteeth,[15] tearing modes,[16] and Alfvén eigenmodes.[17]

The KSTAR ECEI system[12] consists of a pair of independent detector arrays and a large aperture optics as illustrated in Fig. 1(a), providing a simultaneous measurement of two regions in the same poloidal crosssection. The two viewing areas, which correspond to the individual detector arrays as denoted by HFS (high-field side) and LFS (low-field side) in the figure, can be placed anywhere in the poloidal crosssection

[a)]Paper YI2 5, Bull. Am. Phys. Soc. **56**, 359 (2011).
[b)]Invited speaker.

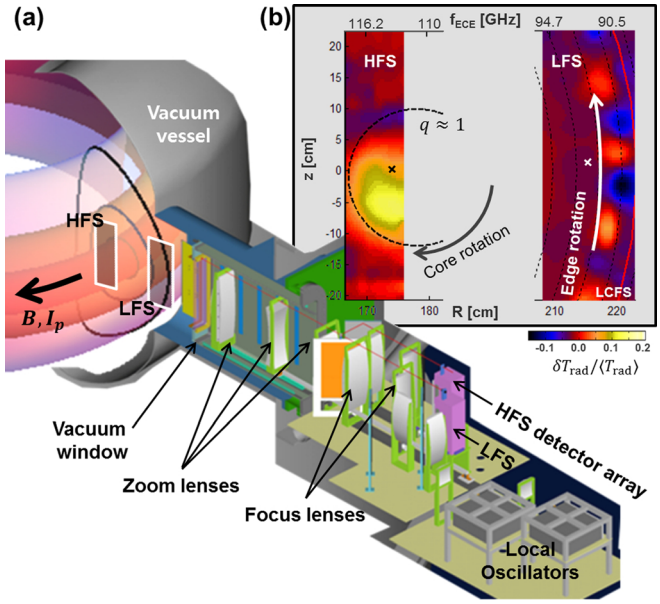

FIG. 1. (a) KSTAR ECEI system. An example combination of high- and low-field side views (HFS and LFS, respectively) are overlaid on the equilibrium flux surfaces for typical H-mode discharges. (b) An example of simultaneous measurement of HFS and LFS (shot# 4362, $t = 1.741863$s). Arrows indicate the direction of apparent rotations. The red curve is the approximate position of the last closed flux surface (LCFS) estimated from an equilibrium reconstruction. The cross marks indicate the positions of the ECEI channels in the time trace of Fig. 2(a).

with a variable vertical coverage from ~30 to ~90 cm owing to the wide-band (85–145 GHz) microwave heterodyne detection technologies[18] and the optimized zooming and focusing capabilities of the optics. This flexibility has allowed various combinations of HFS and LFS view positions, providing excellent opportunities in studying a variety of plasma instabilities and turbulence phenomena in 2D such as sawteeth, tearing modes, ELMs, and turbulent fluctuations during *H*-mode transition.

Each detector array provides 24 (vertical) × 8 (radial) = 192 local $T_{\rm rad}$ measurements with a spatial resolution ~1–2 cm and a time resolution ~1 μs. The detector arrays are optimized for the extraordinary (X-) mode 2nd harmonic ECE at $B_0 = 2$ T (the magnetic field at the major radius $R_0 = 1.8$ m), which is a linearly polarized wave perpendicular to the magnetic field. For high field operations $B_0 > 3$ T, the X-mode 2nd harmonic ECE exceeds the detectable range. Instead, the detection of the parallel-polarized ordinary (O-) mode fundamental ECE has been recently demonstrated using a pair of large-aperture polarization rotators.[19]

Fig. 1(b) shows an example of simultaneous measurement of core and edge instabilities, demonstrating the unprecedented diagnostic capability of the ECEI system. Here, the HFS image shows an internal kink mode in the central region, while the LFS image shows the ELM filaments in the edge. Both images are plotted in the same $\delta T_{rad}/\langle T_{rad}\rangle$ scale, where $\langle T_{rad}\rangle$ denotes a time average and $\delta T_{rad} \equiv T_{rad} - \langle T_{rad}\rangle$. Note that the observed rotation of the ELM filaments is counterclockwise (electron diamagnetic drift direction) in the ECEI view in opposite to the clockwise rotation of the core, indicating a strong flow shear.

The ECE localization as well as the relation $\delta T_{rad}/\langle T_{rad}\rangle = \delta T_e/\langle T_e\rangle$ (or equivalently $T_{rad} \propto T_e$) will hold true in the central region where $\tau \gg 1$. The ECE localization is presumably still valid for the filamentary region as implied by the high contrast and coherent poloidal rotation of the filaments. This assertion can be substantiated by considering the radial τ profile in the edge region for a typical KSTAR *H*-mode[20] according to the approximate formula $\tau \approx 2.5 n_e([10^{19}\mathrm{m}^{-3}])\, T_e([\mathrm{keV}])$(Ref. 14) for the 2nd harmonic X-mode ECE propagating perpendicular to the magnetic field. Even with the conservative values $n_e \gtrsim 1 \times 10^{19}\mathrm{m}^{-3}$ and $T_e \gtrsim 0.5$ keV for the pedestal top, the estimated optical depth is $\tau > 1$ at the left side of the filamentary region, i.e., the pedestal top region because the ELMs are generally believed to develop at the steepest pressure gradient.[2,4] Combined with the observed coherent rotation of the entire filaments in the poloidal direction, this supports the validity of the ECE local measurement for all filament regions. On the other hand, the fluctuation $\delta T_{rad}/\langle T_{rad}\rangle$ will contain the finite density effect in the case of marginal optical depth,[12,13] i.e.,$\delta T_{rad}/\langle T_{rad}\rangle = (1 + A_2)\delta T_e/\langle T_e\rangle + A_2 \delta n_e/\langle n_e\rangle$, where $A_2 = (1 - r)\tau e^{-\tau}/(1 - e^{-\tau})(1 - re^{-\tau})$ and r is the wall reflection coefficient. For example, $A_2 \approx 0.3$ using $\tau = 1$ and $r = 0.6$, and the n_e fluctuation of ~30% will result in the T_{rad} fluctuation of ~9%. A precise physical interpretation of $\delta T_{rad}/\langle T_{rad}\rangle$ is difficult at present due to the uncertainty in the density fluctuation level and the wall reflection coefficient. Near the last closed flux surface (LCFS) and outside, the ECE is not localized any longer and the ECEI measurements become invalid.

III. ELM DYNAMICS—UNPERTURBED CASE

In 2010 KSTAR campaign, ELMy H-mode plasmas were obtained with a moderate auxiliary heating ~1 MW and a strong shaping (elongation ~1.8 and triangularity ~0.6),[20] where a typical sequence of ELM behaviors was observed, i.e., initially small-amplitude ELMs following the H-mode transition, a quiescent period, and large-amplitude ELMs. Fig. 2(a) shows the time traces of the Balmer alpha (D_α) emission, core and edge ECEI signals, and line-averaged electron density ($n_{e,l}$) for a typical H-mode deuterium discharge with co-current neutral beam injection (NBI) ~1 MW (beam energy ~70 keV) and perpendicular electron cyclotron resonance heating (ECRH) ~250 kW (frequency = 110 GHz). The plasma parameters during the H-mode phase were $B_0 = 2$ T, plasma current $I_p = 600$ kA, core T_e ~1 keV, $n_{e,l} \sim 3.5 \times 10^{19}\mathrm{m}^{-3}$, and q_{95} ~6. The H-mode transition as indicated by a large D_α drop at t ~1.23 s was slow due to the marginal heating power compared to typical transitions observed in other tokamaks. Nonetheless, the formation of pedestal was clearly observed in both T_e and T_i profiles, which measured a steep temperature gradient from ~1 keV to ~200 eV in a narrow edge region of ~5 cm.

Fig. 2(b) is the zoomed time traces showing a mix of two different types of ELM events, i.e., small and large crashes. The small crashes, corresponding to the semiperiodic (~2 ms) bumps in the D_α trace, are a single burst of one ELM filament in the ECEI view with negligible change in the pedestal region. In contrast, the large crashes involve a

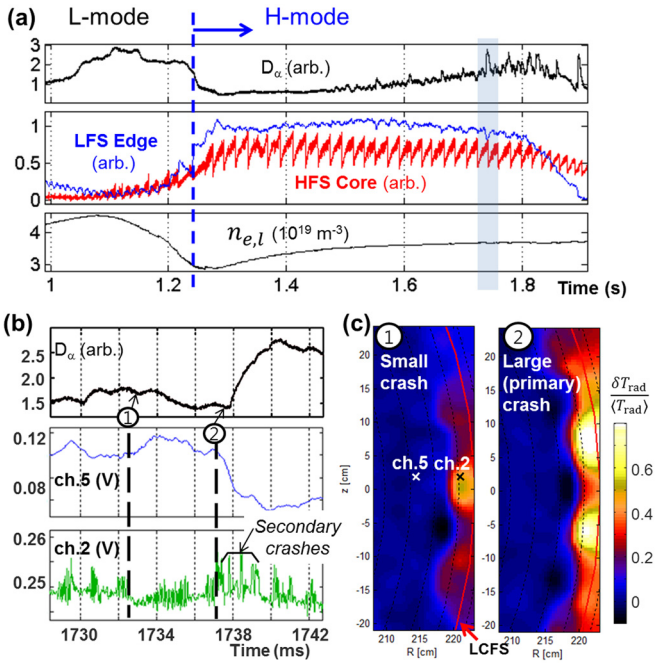

FIG. 2. (a) Time evolution of D_α (lower divertor), core and edge ECEI signals (the channel positions are indicated in Fig. 1(b)), and $n_{e,l}$ for shot# 4362. (b) Detailed time traces of D_α and ECEI channels from near the pedestal top (ch. 5) and the filament region (ch. 2). (c) Examples of small and large ELM crash images.

sharp increase in D_α trace and a significant drop of the pedestal ECE intensity (~5–10%), indicating loss of the edge confinement. In general, a large crash consists of a series of filament bursts, which are similar to the phenomenology of the primary and secondary filaments observed in NSTX (Ref. 9) and C-Mod.[10] The present paper is focused on the ELM evolution and the crash dynamics of large ELM events, which are described by the 2D ECEI images of Figs. 3 and 4.

Fig. 3(a) is the time trace of an ECEI channel at the filament region, illustrating the three distinct evolution phases observed in typical KSTAR ELMy H-mode plasmas: the initial growth stage (time marks 1–4), the interim saturated state (time marks 4–5), and the final crash stage (highlighted time window starting from the time mark 7) through a short transient phase (around the time mark 6).

In the linear growth stage shown in Fig. 3(b), the individual filaments grow in amplitude and extend radially outward across the flux surfaces on the average. The average growth rate estimated by the integrated ECE amplitude of the filament regions (defined by an arbitrary intensity contour level) is semiexponential, implying that the perturbation, presumably the peeling-ballooning mode,[2] is in a linear state. However, the observed growth has substantial fluctuations in both the amplitude and radial extent, which may suggest a toroidal nonuniformity or temporal variation of the growth rate. The apparent poloidal rotation of the filaments, $V^*_{\rm pol} \sim +1$km/s, is counterclockwise (i.e., in the electron diamagnetic drift direction) from the moment of birth. Note that the effect of the toroidal plasma flow $(V_{\rm tor})$ on the apparent filament rotation is clockwise, which implies a net poloidal plasma flow $(V_{\rm pol})$ or phase velocity of the filamentary mode $(V_{\rm ph})$ because $V^*_{\rm pol} = V_{\rm pol} + V_{\rm ph} - V_{\rm tor}\tan\alpha$, where α is the

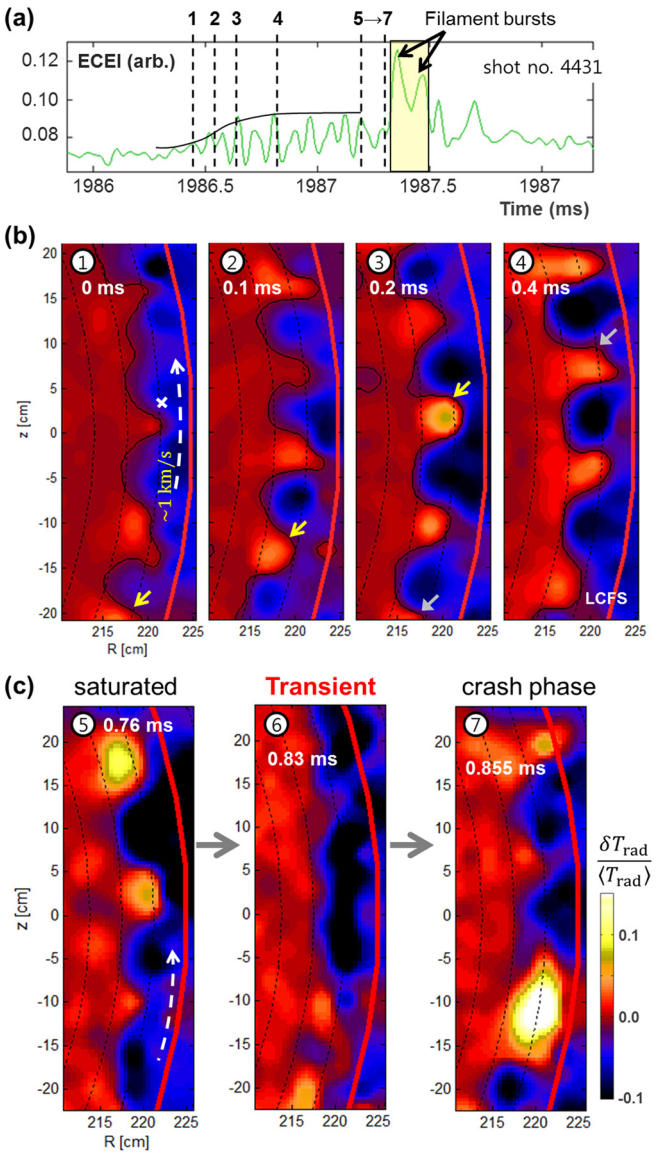

FIG. 3. ELM evolution images (shot# 4431). (a) Time trace of an ECEI channel at the filament region (indicated by the cross mark in the frame 1). (b) Initial growth (frames 1–3) and saturation (frame 4) of multiple ELM filaments. The short arrows identifying individual filaments illustrate the apparent counterclockwise rotation of the filaments (also indicated by the long dashed arrow in frame 1). (c) Changes of the filament structure through a short transient period. All frames are plotted in the same color scale.

pitch angle of the filaments. Clockwise $V^*_{\rm pol}$ was rarely observed, which may imply a critical $V_{\rm pol}$ (or radial electrical field E_r (Refs. 1 and 21)) for the onset of the linear instability. In some cases, $V^*_{\rm pol}$ was intermittent instead of being continuous and the cause of this intermittency is unknown at present.

In the interim saturated state (see frame 4 of Fig. 3(b)), the filamentary instability has grown to a large radial size (~5 cm; the radial span of the deformed contour $\delta T_{rad}/\langle T_{rad}\rangle = 0$). The filamentary structure is regular and quasi-stable without any average growth although individual filaments still maintain the level of fluctuations similar to the growth phase. The time duration of this stage is highly random from being almost absent to several 100 μs. The large

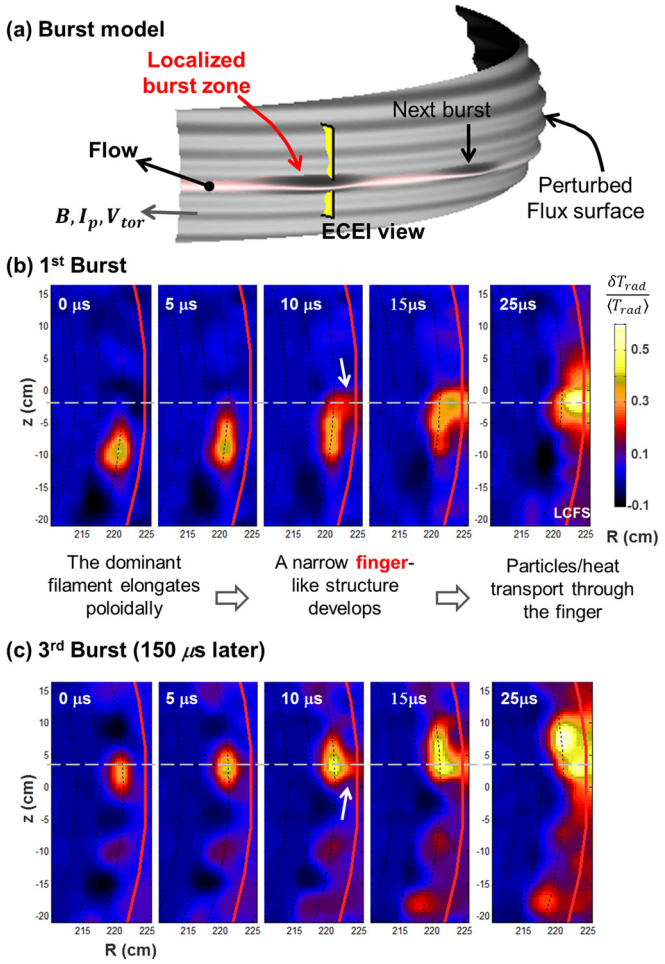

FIG. 4. ELM crash images corresponding to the time window indicated in Fig. 3(a). (a) Phenomenological model for multiple bursts of the same filament. Highlighted is the dominant filament which is undergoing a series of bursts through localized bulges. (b) The first burst in the series of four bursts. The fingerlike bulge is indicated by a short arrow. (c) Third burst of the same filament, 150 μs later.

radial extent, quasistability, and random duration indicate that the initial linear instability has evolved into a metastable nonlinear state[22] with the presence of random perturbations although the underlying stabilization mechanism is not understood yet. As shown in Fig. 3(c), a very short transient period ($\lesssim 50\,\mu$s) has been frequently observed near the end of the saturated state prior to the final crash. The filaments almost disappear from the ECEI view and then reemerge with an irregular structure: usually one filament becomes dominant and the spacing between filaments becomes irregular and larger. The abrupt change in the poloidal mode structure may be important for the crash trigger mechanism, which needs further investigation.

The observed ELM crash process is essentially localized and nonlinear in nature. Fig. 4(a) is a phenomenological model for the crash as a series of localized filament bursts. The highlighted flux tube is the bursting filament where each localized bulge indicates the bursting zone at a specific time. The rotation of the filaments is indicated by an arrow in the laboratory frame. Note the ECEI can capture the exact process of the ELM filament burst only when the localized burst enters the ECEI view, which is located at a single toroidal location as illustrated in the model figure. The detailed sequence of the observed crash process is illustrated by two such examples in Figs. 4(b) and 4(c), which were the first and third bursts in a series of four bursts of the same filament. The two events were clearly isolated events because they were separated in time by $\sim$150 μs, which is much longer than the parallel transport time scale of the thermal electrons once around the torus ($\sim$1 μs) and the toroidal Alfvénic time scale ($\sim$1 μs).

The crash phase starts with the poloidal elongation of the filaments as shown in the first frame of each example. Then, a narrow fingerlike structure develops at one of the filaments as indicated by the arrow in the third frame. This finger corresponds to the localized bulges in the model figure in Fig. 4(a). As this finger extends radially and touches the LCFS, the ECE intensity along the finger and outside the LCFS increases rapidly. This is a clear indication of a particle-heat flux through the finger. The dominant flux in the radial direction, lasting for $\sim$50 μs or less, is localized and convective rather than diffusive, which suggests that the underlying mechanism of the ELM filament eruption may be similar to the pressure-driven localized burst and collective heat transport in the sawtooth crashes.[15] Interestingly, the poloidal rotation of the bursting filament slows down at the finger location as indicated by the dashed line in each example, while the rest of the filament keeps moving at the same speed. A magnetic reconnection may be responsible for this slowing-down or braking of the finger as well as the collective heat transport. The existence of magnetic reconnection is supported by a preliminary observation of broadband low frequency rf radiation in the range of Alfvén-whistler waves ($<$ 3 GHz) synchronized with individual filament bursts.[23,24] Note that the toroidally and poloidally localized filament burst, consistent with the finger-initiated crash, is also supported by other seemingly different observations characterized by a sudden heat pulse appearing from outside the LCFS and spreading over the entire filament region within 10 μs, which would correspond to the ELM filament bursts occurring away from the ECEI view.

IV. ELM DYNAMICS UNDER n = 1 MAGNETIC PERTURBATION

In 2011 KSTAR campaign, ELMy H-mode plasmas were obtained with higher total auxiliary heating power ($\sim$1.4 MW 90 keV NBI, $\sim$300 kW 110 GHz ECRH, and $\sim$300 kW 170 GHz ECRH), resulting in baseline ELMs with higher crash amplitudes than those of the "large" ELMs in 2010. The effect of external magnetic perturbations (MPs) with the toroidal mode number $n = 1$ on the ELM behaviors have been investigated using three sets of field error correction coils. Further details on the ELM control experiments can be found elsewhere.[25]

Fig. 5(a) is an example of D_α time trace for a typical H-mode discharge with an n = 1 MP, showing that the MP initially intensifies the ELM crash and then leads to suppression. Here, the three labels indicate (1) the baseline period prior to the MP, (2) the intermediate ELM-intensified period where the MP had both non-resonant and resonant

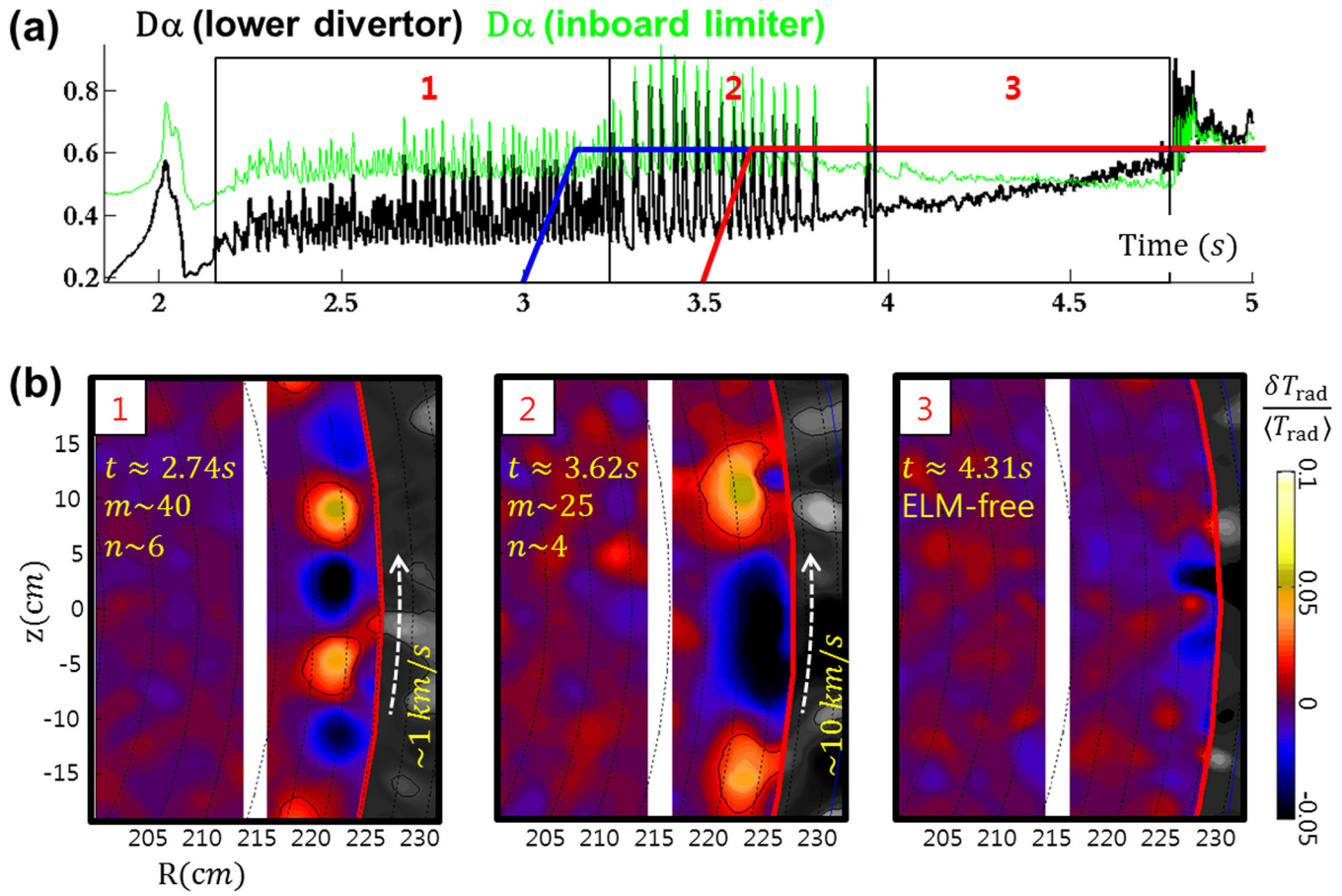

FIG. 5. Alteration of ELM dynamics under n=1 MP (shot# 6123). (a) Time trace of D_α emissions [lower divertor (lower thick line) and inboard limiter (thin green line)] showing the changes in frequency and amplitude of the ELM crash events. The blue and red lines indicate the MP pulses, where the combination of both produces a resonant perturbation. (b) ECEI images of the edge region, showing (1) typical ELM structure before RMP, (2) altered ELM structure after the application of MP, and (3) no filamentary structure during the ELM-free phase.

components with respect to the local magnetic field lines, and (3) the ELM-free period where the MP was mostly resonant. The corresponding ECEI images in Fig. 5(b) shows substantial alterations of ELM dynamics such as filament spacing, poloidal rotation, and crash pattern. Note the first two ECEI images show the ELM filaments in the pre-crash phase.

In period 1, the ELM structure and dynamics are identical to the previous "large" ELM case; the conspicuous ELM filament structure with similar size and poloidal spacing, the poloidal rotation of the same order (V^*_{pol}~1 km/s), and the crash through a series of localized filament bursts. The pre-crash ELM filaments exist for ~15 ms, significantly longer than the previous case (~1 ms), which may be related to the absence of "small" ELM crashes. In period 2, substantial changes have been observed in all aspects of the ELM evolution. The spacing between the filaments has been increased, suggesting a reduction in the poloidal and toroidal mode numbers (m and n, respectively). The estimated mode numbers[13] are compared in the figure between the periods 1 and 2. Interestingly, the apparent poloidal rotation of the filaments (V^*_{pol}~10 km/s) is much faster than the previous period by a factor of 10. The mechanism of the MP-induced V^*_{pol} enhancement is important for the ELM dynamics and currently under investigation. These pre-crash ELM filaments exist only for a short period time ~1 ms with a monotonic decrease both in the filament amplitude and V^*_{pol}. In addition, the crash is a single burst with higher amplitude rather than multiple bursts. In period 3, the ELM filaments have disappeared and the plasma is free of major transport events leading to a pedestal collapse. Instead, tiny transport events with no pedestal change have been observed occasionally with a transient pre-cursor phase (~10 μs) showing a non-rotating filamentary structure. The tiny transport events may be critical to the understanding of the MP-induced ELM suppression.

V. SUMMARY

In summary, the entire nonlinear evolution process of filamentary ELM structures has been studied in 2D using the ECEI system. The three-stage ELM evolution consists of the linear growth, the quasisteady saturated state, and the crash. The initial growth of the multiple ELM filaments is exponential in time and strongly localized in the edge region, which is in qualitative agreement with the linear peeling-ballooning model.[2] The saturated state is meta-stable but eventually transforms into the final crash phase through a short transient phase. The large ELM crash event is a series of filament bursts, which are inherently 3D and nonaxisymmetric events localized both poloidally and toroidally. Substantial alterations in these ELM dynamics under n = 1 magnetic

perturbations have been observed, shedding light into the ELM suppression mechanism via magnetic perturbations.

ACKNOWLEDGMENTS

We thank Professor Steve Sabbagh and Dr. Young-Seok Park for providing the equilibrium flux surface reconstructions despite lack of appropriate kinetic profile measurements. We also thank Professor Patrick Diamond and Dr. Linda Sugiyama for providing theoretical and simulation perspectives on the ELM filament dynamics and Professor Paul Bellan for discussions on the magnetic reconnection physics in the context of ELM crashes. This work was performed under the auspices of the NRF Korea, the US DOE, and the Euratom-FOM association.

[1]F. Wagner, Plasma Phys. Controlled Fusion **49**, B1 (2007).
[2]P. B. Snyder, H. R. Wilson, J. R. Ferron, L. L. Lao, A. W. Leonard, T. H. Osborne, A. D. Turnbull, D. Mossessian, M. Murakami, and X. Q. Xu, Phys. Plasmas **9**, 2037 (2002).
[3]E. J. Doyle, Nucl. Fusion, **47**, S18 (2007).
[4]P. B. Snyder, H. R. Wilson, T. H. Osborne, and A. W. Leonard, Plasma Phys. Controlled Fusion **46**, A131 (2004).
[5]A. Kirk, B. Koch, R. Scannel, H. R. Wilson, G. Counsell, J. Dowling, A. Herrmann, R. Martin, M. Walsh, and the MAST team, Phys. Rev. Lett. **96**, 185001 (2006).
[6]A. Kirk, T. Eich, A. Herrmann, H. W. Muller, L. D. Horton, G. F. Counsell, M. Price, V. Rohde, V. Bobkov, B. Kurzan, J. Neuhauser, H. Wilson, and the ASDEX Upgrade and MAST Teams, Plasma Phys. Controlled Fusion, **47**, 995 (2005).
[7]C. Silva, W. Fundamenski, A. Alonso, B. Gonçalves, C. Hidalgo, M. A. Pedrosa, R. A. Pitts, M. Stamp, and JET-EFDA contributors, Plasma Phys. Controlled Fusion, **51**, 105001 (2009).
[8]J. A. Boedo *et al.*, Phys. Plasmas **12**, 072516 (2005).
[9]R. J. Maqueda, R. Maingi, and NSTX team, Phys. Plasmas **16**, 056117 (2009).
[10]J. L. Terry, I. Cziegler, A. E. Hubbard, J. A. Snipes, J. W. Hughes, M. J. Greenwald, B. LaBombard, Y. Lin, P. Phillips, and S. Wukitch, J. Nucl. Mater. **363–365**, 994 (2007).
[11]G. S. Lee *et al.*, Nucl. Fusion **40**, 575 (2000).
[12]G. S. Yun, W. Lee, M. J. Choi, J. B. Kim, H. K. Park, C. W. Domier, B. Tobias, T. Liang, X. Kong, N. C. Luhmann, Jr., and A. J. H. Donné, Rev. Sci. Instrum. **81**, 10D930 (2010).
[13]G. S. Yun, W. Lee, M. Choi, J. Lee, H. K. Park, B. Tobias, C. W. Domier, N. C. Luhmann, Jr., A. J. H. Donné, J. H. Lee, and KSTAR team, Phys. Rev. Lett. **107**, 045004 (2011).
[14]M. Bornaciti, R. Cano, O. De Barbieri, and F. Engelmann, Nucl. Fusion **23**, 1153 (1983).
[15]H. K. Park, N. C. Luhmann, Jr., A. J. H. Donné, I. G. J. Classen, C. W. Domier, E. Mazzucato, T. Munsat, M. J. van de Pol, Z. Xia, and TEXTOR team, Phys. Rev. Lett. **96**, 195003 (2006).
[16]I. G. J. Classen, E. Westerhof, C. W. Domier, A. J. H. Donné, R. J. E. Jaspers, N. C. Luhmann, Jr., H. K. Park, M. J. van de Pol, G. W. Spakman, M. W. Jakubowski, and the TEXTOR team, Phys. Rev. Lett. **98**, 035001 (2007).
[17]B. J. Tobias, I. G. J. Classen, C. W. Domier, W. W. Heidbrink, N. C. Luhmann, Jr., R. Nazikian, H. K. Park, D. A. Spong, and M. A. Van Zeeland, Phys. Rev. Lett. **106**, 075003 (2011).
[18]B. Tobias, C. W. Domier, T. Liang, X. Kong, L. Yu, G. S. Yun, H. K. Park, I. G. J. Classen, J. E. Boom, A. J. H. Donné, T. Munsat, R. Nazikian, M. Van Zeeland, R. L. Boivin, and N. C. Luhmann, Jr., Rev. Sci. Instrum. **81**, 10D928 (2010).
[19]J. Lee, G. S. Yun, M. Kim, W. Lee, and H. K. Park, "Large-aperture broadband polarization rotator for the KSTAR ECE imaging system," J. Instrum. **7**, C01037 (2012).
[20]S.W. Yoon *et al.*, Nucl. Fusion **51**, 113009 (2011).
[21]K. H. Burrell, Phys. Plasmas **6**, 4418 (1999).
[22]H. R. Wilson and S. C. Cowley, Phys. Rev. Lett. **92**, 175006 (2004).
[23]J. Leem, G. S. Yun, and H. K. Park, "Fast RF spectrometer for MHD event detection," J. Instrum. **7**, C01042 (2012).
[24]P. M. Bellan, Phys. Plasmas **5**, 3081 (1998).
[25]Y. M. Jeon *et al.*, "Suppression of edge localized modes in high-confinement KSTAR plasmas by non-axisymmetric magnetic perturbations," Phys. Rev. Lett. (submitted).